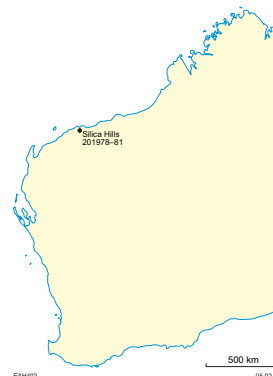


201981: gold-bearing nodule, Silica Hills (Tozer Formation, Sholl Terrane)

Sample type	Gold-bearing nodule
Sample mass	4.1 g
Sample location	Silica Hills, about 25 km south of Karratha
Coordinates	Zone 50, MGA 492350E 7684225N
Datum	GDA94
1:250 000 map sheet	DAMPIER (SF 50-2)
1:100 000 map sheet	DAMPIER (2256)
Tenement	M 47/232
Collector	Artemis Resources Limited



Location and sampling

The sample was provided by Artemis Resources Limited in January 2019. It was collected from the weathering profile above quartz-veined felsic volcanic rocks at the Silica Hills prospect, in the northwest Pilbara region (Artemis Resources Limited, 2019, written comm., 11 January).

Geological context

The Silica Hills prospect is located about 4 km south of the Sholl Shear Zone, a significant terrane boundary in the Sholl greenstone belt of the Sholl Terrane of the northwest Pilbara Craton (Hickman, 2016; GSWA, 2020). The local bedrock comprises metamorphosed rhyolite and dacite of the 3128–3116 Ma Tozer Formation (compiled out of the GSWA 1: 100 000 scale geology map). Metamorphosed basalt and basaltic andesite of the Tozer Formation (Hickman, 2021) outcrop immediately north of the sample locality. Proterozoic dolerite dykes transect the area (GSWA, 2020).

Gold mineralization in the area typically consists of residual to eluvial and alluvial gold (e.g. Sholl Northeast 2 Eluvial, Mt Sholl Dryblowing 1, Mt Sholl B1 East [Cu], Specimen and Silica Hills). Eluvial gold and gold-in-soil geochemical anomalies appear to have been derived from small, shallow dipping quartz veins along lithological contacts (Bob Clyne and Associates, 1988). High grade gold mineralization discovered in 2017 by Artemis Resources Limited at Silica Hills consists of coarse nuggetty gold with high silver content in a quartz -vein stockwork within a silicified intrusion along a shear zone (Artemis Resources Limited, 2017).

The nearest regolith landforms are a colluvial unit comprising unconsolidated sand, silt, and gravel in outwash fans, scree, talus, and an alluvial–fluvial unit comprising unconsolidated sand, silt, and gravel in active but poorly defined drainage channels on floodplains (GSWA, 2020).

Methodology

The sample was photographed and weighed, and its overall morphology and external features, such as colour, roundness, surface relief, coatings, mineral inclusions and mineralogical assemblages were recorded using visual morphometry. A subsample containing a gold grain was cut from the main specimen and analysed by using scanning electron microscopy with energy dispersive X-ray system (SEM-EDS). The subsample was then mounted in epoxy resin and polished, and the gold microstructure and inclusions were examined using reflected-light microscopy and SEM-EDS. Gold microchemistry was determined by laser ablation inductively coupled plasma mass spectrometry (LA-ICP-MS), calibrated against certified gold reference materials (CRM; Murray, 2009). The sample was ablated in triplicate along 0.5 mm-long traverses and average values calculated for elements present in the CRM. The gold surface was repolished after laser ablation, and etched with aqua regia, but this failed to reveal the internal structure due to extensive reaction of the acid with calcareous clays. The surface was therefore clean and repolished using ion beam milling, and the nugget microstructure verified using electron back-scattered diffraction (EBSD). Details of this method are described in Hancock and Beardsmore (2020).

Morphology

The primary sample is a nodule 20 mm in diameter, comprising abundant small, rounded quartz grains and an irregularly shaped, 8 × 5 mm gold grain, in a ferruginous clay matrix (Fig. 1).

SEM-EDS analysis of raw surfaces

Gold and quartz grains were both detected on the nodule surface, and organic (plant) material and Si–Al–Fe±K clays (Fig. 2a). The surface of the gold grain is spongy, scratched and pitted, but not compacted (Fig. 2b).

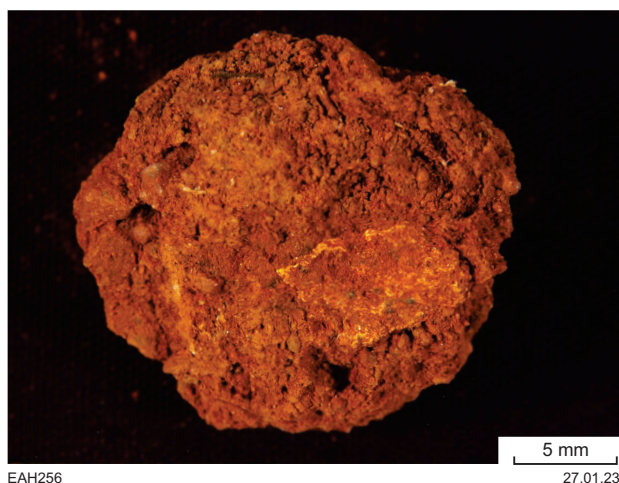


Figure 1. Sample 201981: gold-bearing nodule, Silica Hills prospect

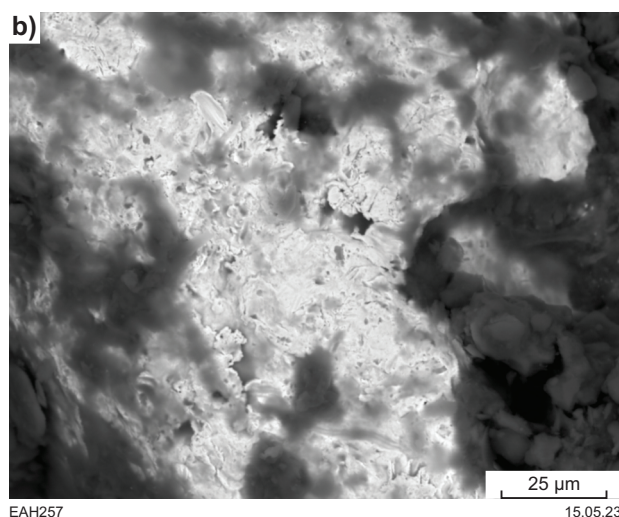
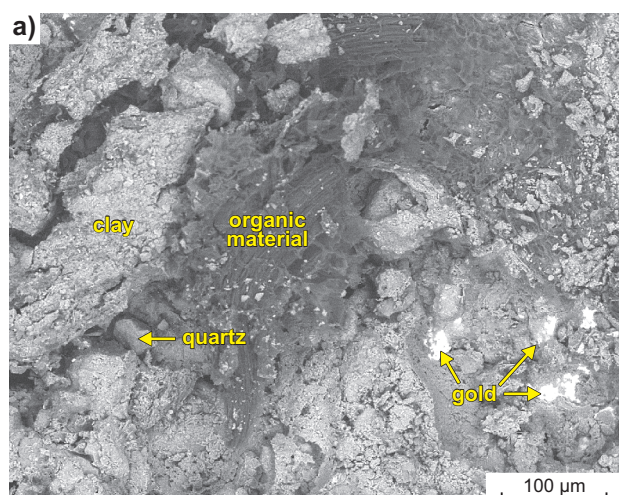


Figure 2. Backscattered electron images of parts of surface of sample 201981: gold-bearing nodule, Silica Hills prospect: a) nodule; b) gold grain

Optical microscopy of polished surfaces

The irregular shape and solution-pitted surface of the gold nugget is clearly evident in polished section, as are many large cracks and voids that penetrate the grain and are now filled with ferruginous clays and small quartz grains (Fig. 3a). Thin veinlets of Ag-free gold are common around voids, and there are also small, irregular galena inclusions within the grain (Fig. 3b). Gold nanoparticles are disseminated in regolith inclusions, in some instances preferentially along planar fabrics, or along their margins that are in contact with coarse gold (Figs. 3c, d).

SEM-EDS analysis of polished surfaces

The bulk of the gold grain contains 22% Ag, but narrow intergranular veinlets and finely disseminated gold contain no Ag. The presence of small galena inclusions was confirmed, as were void-filling Mg–Al–Si–Fe–K clays containing finely disseminated gold (Fig. 4a). Preferentially aligned platy or discoidal nanoparticles of pure gold are distributed within a mass of chlorite–illite clay believed to be an altered K-feldspar inclusion (Fig. 4b).

LA-ICP-MS analysis

Ag, Cu and Hg were consistently detected within the gold grain in concentrations higher than the instrument detection limit, and probably occur as limited solid solutions in the gold. The bulk of the gold grain contains high Ag (16–18%, a little lower than determined by SEM-EDS spot analysis), and low concentrations of Cu (52–68 ppm) and Hg (88–94 ppm; Table 1). Mg, Fe, Sb, Bi, and Pb were detected only sporadically in concentrations, under detection limits (sub-ppm; Table 2), while Al relative contents (in cps) are very high. All these elements are occurring in micro- and nano-inclusions.

SEM-EBSD analysis

Etching with aqua regia failed to produce a useable surface due to strong reaction with possible calcareous clays and Ag. The cut surface was therefore etched using ion-beam milling and analysed using SEM-EBSD. This revealed a poly-crystalline fabric with many polysynthetic and simple twinning planes, with coherent and incoherent, rounded, smooth or irregular crystal boundaries. The grain size is smaller around some voids and inclusions (Fig. 5). The microstructure indicates complete recrystallization sometime after primary gold precipitation.

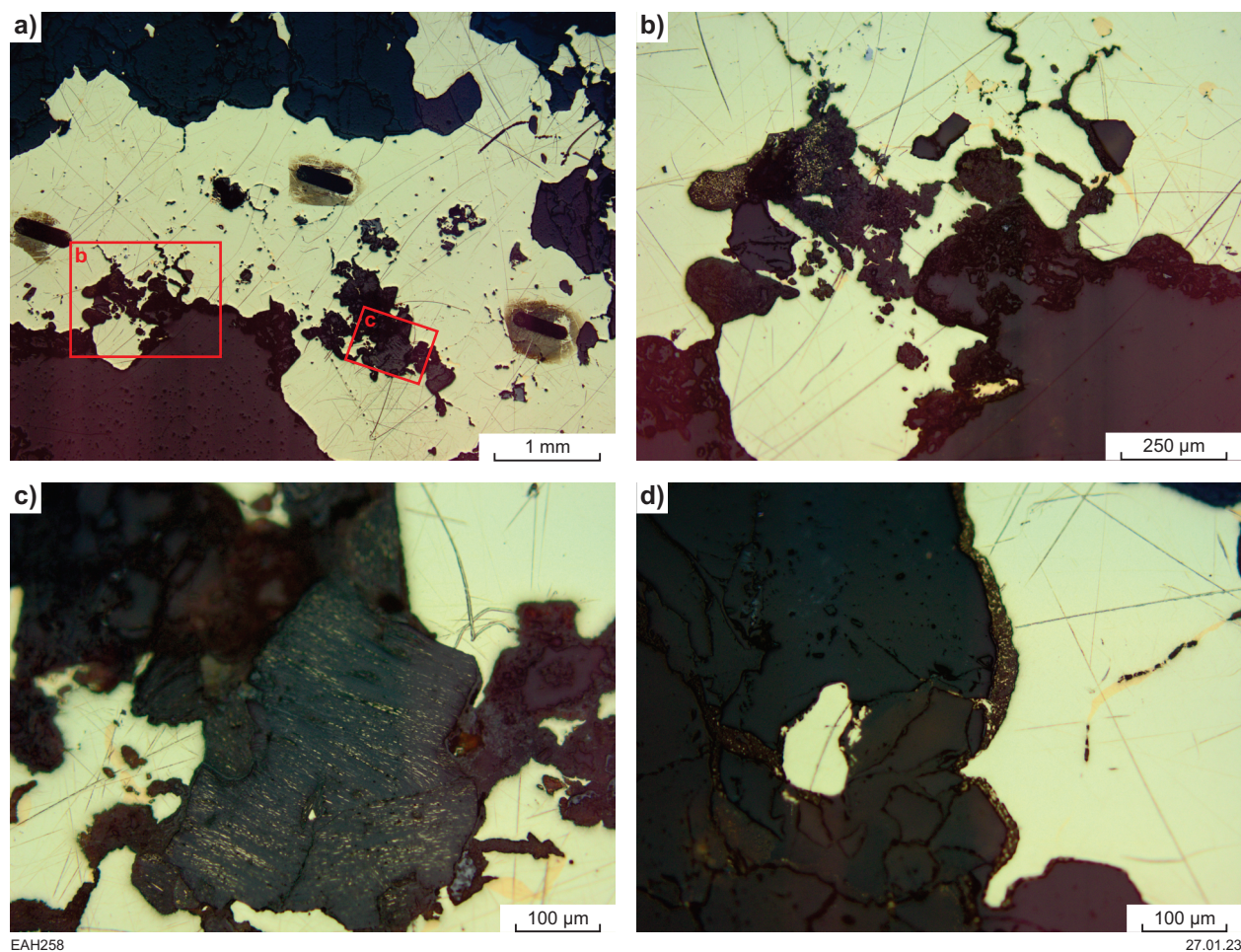


Figure 3. Reflected-light photomicrographs of cut and polished surface of gold grain extracted from sample 201981: gold-bearing nodule, Silica Hills prospect. Dark, elongate lines are laser ablation tracks produced during LA-ICP-MS

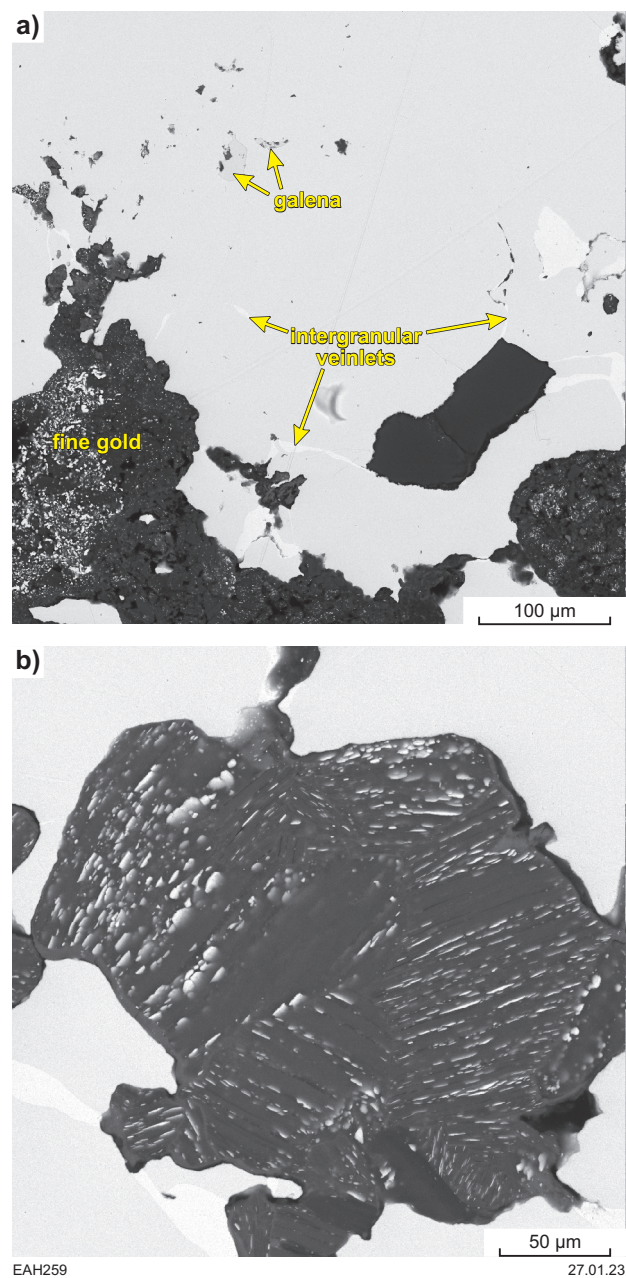


Figure 4. Backscattered electron images of polished surface of gold grain extracted from sample 201981: gold-bearing nodule, Silica Hills prospect

Table 1. LA-ICP-MS data for main elements (above detection limit) in three traverses in gold grain extracted from sample GSWA 201981: gold bearing nodule, Silica Hills prospect

Ag (%)	Cu (ppm)	Hg (ppm)	Other elements (ppm ¹) ²
16	52	88	
16	59	93	
18	68	94	

NOTES: 1 see Table 2 for concentrations and detection limit
2 results are only shown where standards are available for the element

Table 2. LA-ICP-MS compositional data for gold grain extracted from sample GSWA 201981: gold-bearing nodule, Silica Hills prospect

Laser ablation track	Unit	⁷ Li	⁹ Be	¹¹ B	²³ Na	²⁵ Mg	²⁷ Al	²⁹ Si	⁴⁴ Ca	⁴⁵ Sc	⁴⁹ Ti	⁵¹ V	⁵³ Cr	⁵⁵ Mn	⁵⁷ Fe	⁵⁹ Co	⁶⁰ Ni	⁶⁵ Cu
1	cps					44	383			14	2		4			2		6400
2	cps					230	2109			22	3		9	13	71	35	31	7294
3	cps			50		153	36156		11		6	7	5		96	7	4	8372
1	ppm					0.53					0.04							52
2	ppm					2.75					0.05						0.31	59
3	ppm					1.83					0.13						0.04	68
DL*	ppm					3.3					1.5		1.7	1.1	3.4		2.9	1.5
Laser ablation track	Unit	⁶⁶ Zn	⁶⁹ Ga	⁷² Ge	⁷⁵ As	⁸² Se	⁸⁵ Rb	⁸⁸ Sr	⁸⁹ Y	⁹⁰ Zr	⁹³ Nb	⁹⁸ Mo	¹⁰¹ Ru	¹⁰³ Rh	¹⁰⁸ Pd	¹⁰⁹ Ag	¹¹¹ Cd	¹¹⁵ In
1	cps	7	1				2	4		2	7		1		2	31993622		2
2	cps	17	4	4				9		3	19	1	3		7	31966765		1
3	cps	27	7	3			6	11	6	15	11				8	37829032		
1	ppm	0.07													0.02	155233		
2	ppm	0.19													0.05	155103		
3	ppm	0.31													0.06	183547		
DL*	ppm	5.3			2	3.1								1.5	1.8	2.4		
Laser ablation track	Unit	¹²⁰ Sn	¹²¹ Sb	¹²⁶ Te	¹³³ Cs	¹³⁸ Ba	¹³⁹ La	¹⁴⁰ Ce	¹⁴¹ Pr	¹⁴⁵ Nd	¹⁵¹ Eu	¹⁵⁷ Gd	¹⁵⁹ Tb	¹⁶² Dy	¹⁶⁵ Ho	¹⁶⁷ Er	¹⁶⁹ Tm	¹⁷² Yb
1	cps	18	185	1	2	3				3							2	1
2	cps	12	177	2	2	5				1	1						1	1
3	cps	14	253	2	3	20	3			1		2		2				2
1	ppm	0.08	0.72	0.02														
2	ppm	0.05	0.69	0.03														
3	ppm	0.06	0.98	0.03														
DL*	ppm	1.6	2.8	5.6														
Laser ablation track	Unit	¹⁷⁵ Lu	¹⁷⁸ Hf	¹⁸¹ Ta	¹⁸² W	¹⁸⁵ Re	¹⁸⁹ Os	¹⁹³ Ir	¹⁹⁵ Pt	²⁰² Hg	²⁰⁵ Tl	²⁰⁸ Pb	²⁰⁹ Bi	²³² Th	²³⁸ U			
1	cps			3				1		25564		11	70					
2	cps			1	1					26829		191	17					
3	cps			2			2			27163		44	50		1			
1	ppm									88		0.03	0.15					
2	ppm									93		0.60	0.04					
3	ppm									94		0.14	0.11					
DL*	ppm							2.5	2.5			1.5	2.2					

NOTES: cps, count per second; ppm, parts per million; DL, detection limit

*Detection limits have been determined using AuRM Reference Gold Standards (London Bullion Market Association). Standards were analysed nine times each and an average 2σ (95% Confidence Interval) Limit of Detection determined. Some results given in the text are quoted as values that are below the detection limit for these analytes. These values must be considered as "for information" only.

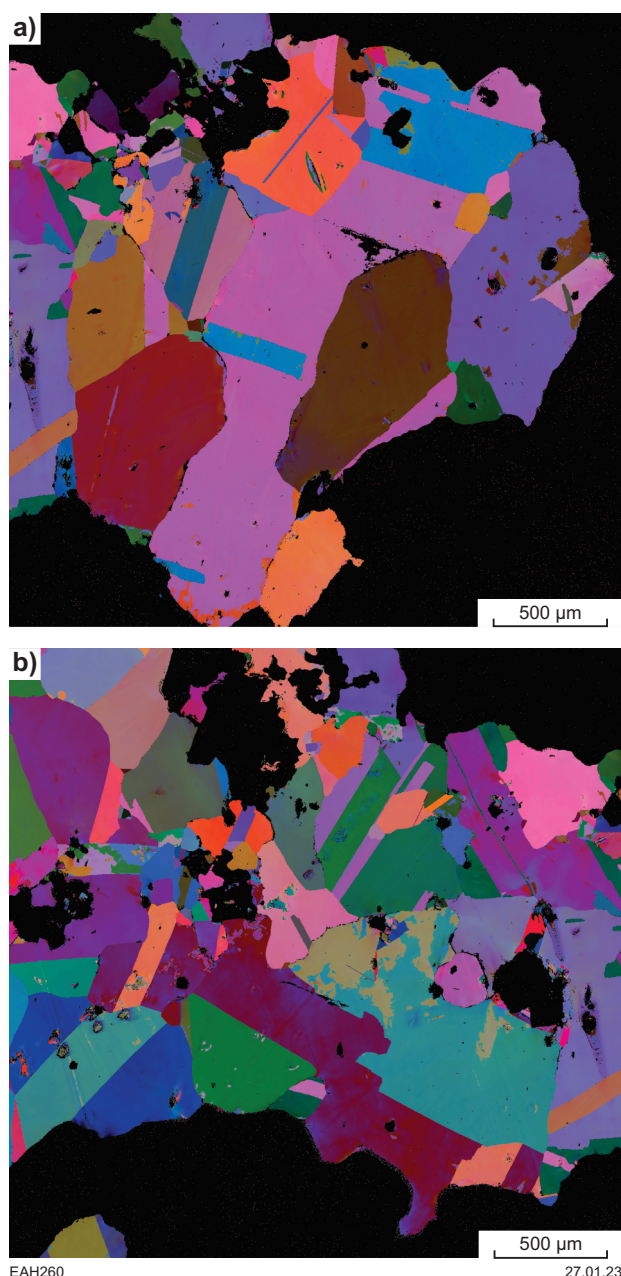


Figure 5. Electron back-scattered diffraction (EBSD) images of parts of repolishing surface of gold grain extracted from sample 201981: gold-bearing nodule, Silica Hills prospect

Interpretation

Primary hydrothermal gold has high Ag and low Cu and Hg abundances, and with small inclusions of galena. There was complete recrystallization of the grain during later deformation, possibly accompanied by some depletion of trace elements, while it was still deep in the crust. The nugget was subsequently released to the surface by uplift and erosion, then buried in the regolith, where the narrow, Ag-free intergranular veinlets have formed during weathering.

Acknowledgements

The authors gratefully acknowledge Michael Verrall (CSIRO) for his help with the SEM/EDS/EBSD operation and data interpretation, and samples preparation for EBSD analysis. We thank Professor John Watling for discussions to improve the LA-ICP-MS data interpretation.

References

- Artemis Resources Limited 2017, High Grade Gold Mineralisation identified at Silica Hills; Karratha, Western Australia (media release): Australian Securities Exchange (ASX), released 28 August 2017, 6p.
- Bob Clyne and Associates 1988, Brady's Prospect, Final Surrender Report for the period 21/02/1986 to 29/06/1990, P47/400 prepared for Mr R Brady: Geological Survey of Western Australia, Statutory mineral exploration report A27188, <www.dmirs.wa.gov.au/wamex>, 58p.
- Geological Survey of Western Australia 2020, Northwest Pilbara, 2020: Geological Survey of Western Australia, Geological Information Series, data package (USB).
- Hancock, EA and Beardsmore, TJ 2020, Provenance fingerprinting of gold from the Kurnalpi Goldfield. Geological Survey of Western Australia Report 212, 21p.
- Hickman, AH 2016, Northwest Pilbara Craton: A record of 450 million years in the growth of Archean continental crust: Geological Survey of Western Australia, Report 160, 104p.
- Hickman, AH 2021, Tozer Formation Formation (A-WHT-xb-f): Geological Survey of Western Australia, WA Geology Online, Explanatory Notes extract, viewed 04 January 2023, <www.dmirs.wa.gov.au/ens>.
- Murray, S 2009, LBMA certified reference materials. Gold project final update: The London Bullion Market Association, Alchemist, no. 55, p. 11–12.

Recommended reference for this publication

Hancock, EA, Blay, OA and Beardsmore, TJ 2025, 201981: gold-bearing nodule, Silica Hills prospect; GSWA Mineralogy Record 15: Geological Survey of Western Australia, 6p.